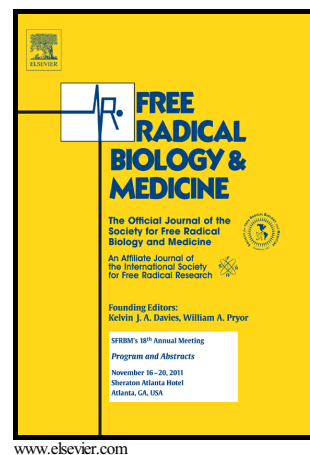


Author's Accepted Manuscript

Sodium butyrate attenuates diabetes-induced aortic endothelial dysfunction via P300-mediated transcriptional activation of *Nrf2*

Junduo Wu, Ziping Jiang, Haina Zhang, Wenzhao Liang, Wenlin Huang, Huan Zhang, Ying Li, Zhaohui Wang, Junnan Wang, Ye Jia, Bin Liu, Hao Wu



PII: S0891-5849(18)31145-6
DOI: <https://doi.org/10.1016/j.freeradbiomed.2018.06.034>
Reference: FRB13830

To appear in: *Free Radical Biology and Medicine*

Received date: 25 November 2017
Revised date: 13 June 2018
Accepted date: 27 June 2018

Cite this article as: Junduo Wu, Ziping Jiang, Haina Zhang, Wenzhao Liang, Wenlin Huang, Huan Zhang, Ying Li, Zhaohui Wang, Junnan Wang, Ye Jia, Bin Liu and Hao Wu, Sodium butyrate attenuates diabetes-induced aortic endothelial dysfunction via P300-mediated transcriptional activation of *Nrf2*, *Free Radical Biology and Medicine*, <https://doi.org/10.1016/j.freeradbiomed.2018.06.034>

This is a PDF file of an unedited manuscript that has been accepted for publication. As a service to our customers we are providing this early version of the manuscript. The manuscript will undergo copyediting, typesetting, and review of the resulting galley proof before it is published in its final citable form. Please note that during the production process errors may be discovered which could affect the content, and all legal disclaimers that apply to the journal pertain.

Sodium butyrate attenuates diabetes-induced aortic endothelial dysfunction via P300-mediated transcriptional activation of *Nrf2*

Junduo Wu¹, Ziping Jiang², Haina Zhang³, Wenzhao Liang⁴, Wenlin Huang⁵, Huan Zhang⁶, Ying Li⁷, Zhaohui Wang⁸, Junnan Wang¹, Ye Jia⁹, Bin Liu^{1,*}, Hao Wu^{2,10,*}.

¹Department of Cardiology, The Second Hospital of Jilin University, 218 Ziqiang St., Changchun, Jilin, 130041, People's Republic of China

²Department of Hand and Foot Surgery, The First Hospital of Jilin University, 71 Xinmin St, Changchun, Jilin, 130021, People's Republic of China

³Department of Rehabilitation, The Second Hospital of Jilin University, 218 Ziqiang St., Changchun, Jilin, 130041, People's Republic of China

⁴Department of Neurology, China-Japan Union Hospital of Jilin University, Changchun, China, 126 Xiantai St, Changchun, Jilin, 130033, People's Republic of China

⁵School of Science and Technology, Georgia Gwinnett College, Lawrenceville, Georgia, 30043, USA

⁶Operating theatre, China-Japan Union Hospital of Jilin University, Changchun, China, 126 Xiantai St, Changchun, Jilin, 130033, People's Republic of China

⁷Department of Dermatology, Affiliated Hospital of Beihua University, 12 Jiefang Rd., Jilin, Jilin, 132000, People's Republic of China

⁸Department of Acupuncture and Tuina, Changchun University of Chinese Medicine, 1035 Boshuo Rd, Changchun, Jilin, 130117, People's Republic of China

⁹Department of Nephrology, The First Hospital of Jilin University, 71 Xinmin St., Changchun, Jilin, 130021, People's Republic of China

¹⁰Department of Translational Medicine, The First Hospital of Jilin University, 71 Xinmin St., Changchun, Jilin, 130021, People's Republic of China

**Corresponding author who handles the article:* Hao Wu, M.D., Ph.D. Department of Hand and Foot Surgery, The First Hospital of Jilin University, 71 Xinmin St, Changchun, Jilin, 130021, People's Republic of China; Department of Translational Medicine, The First Hospital of Jilin University, 71 Xinmin St., Changchun, Jilin, 130021, People's Republic of China. Phone: +86 17390062119. E-mail: wuhaobaha@jlu.edu.cn

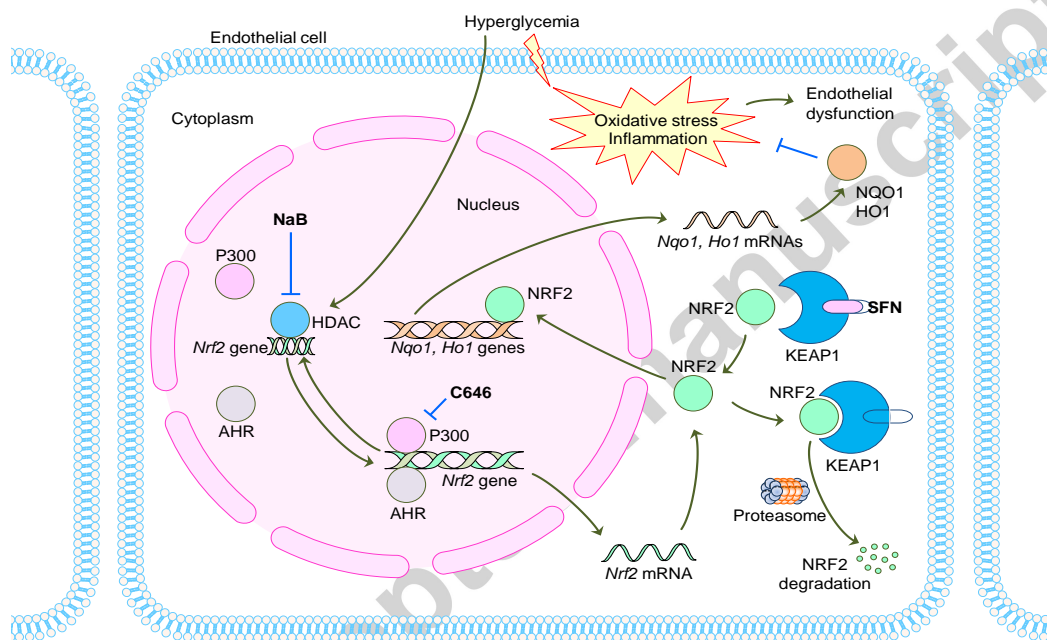
* *Corresponding author:* Bin Liu, M.D., Ph.D., Department of Cardiology, The Second Hospital of Jilin University, 218 Ziqiang St., Changchun, Jilin, 130041, People's Republic of China. Phone: +86 13500810268. E-mail: liubin3333@vip.sina.com

Abstract

Oxidative stress and inflammation are major contributors to diabetes-induced endothelial dysfunction which is the critical first step to the development of diabetic macrovascular complications. Nuclear factor erythroid 2-related factor 2 (NRF2) plays a key role in combating diabetes-induced oxidative stress and inflammation. Sodium butyrate (NaB) is an inhibitor of histone deacetylase (HDAC) and an activator of NRF2. However, NaB's effect on diabetes-induced aortic injury was unknown. It was also not known whether or to what extent NRF2 is required for both self-defense and NaB's protection in the diabetic aorta. Additionally, the mechanism by which NaB activates NRF2 was unclear. Therefore, C57BL/6 *Nrf2* knockout (KO) and wild type (WT) mice were induced to diabetes by streptozotocin, and were treated in the presence or absence of NaB, for 20 weeks. The KO diabetic mice developed more severe aortic endothelial oxidative stress, inflammation and dysfunction, as compared with the WT diabetic mice. NaB significantly attenuated these effects in the WT, but not the KO, mice. In high glucose-treated aortic endothelial cells, NaB elevated *Nrf2* mRNA and protein without facilitating NRF2 nuclear translocation, an effect distinct from that of sulforaphane. NaB

inhibited HDAC activity, and increased occupancy of the transcription factor aryl hydrocarbon receptor and the co-activator P300 at the *Nrf2* gene promoter. Further, the P300 inhibitor C646 completely abolished NaB's efficacies. Thus, NRF2 is required for both self-defense and NaB's protection against diabetes-induced aortic endothelial dysfunction. Other findings suggest that P300 mediates the transcriptional activation of *Nrf2* by NaB.

Graphical abstract



Abbreviations

3-NT, 3-nitrotyrosine; 4-HNE, 4-hydroxynonenal; ACh, acetylcholine; AHR, aryl hydrocarbon receptor; ChIP, chromatin immunoprecipitation; c-NRF2, cytosolic NRF2; Ctrl, control; DM, diabetes mellitus; EC, endothelial cell; HDAC, histone deacetylase; HG, high glucose; HO1, heme oxygenase 1; ICAM-1, intercellular adhesion molecule-1; IHC, immunohistochemical; *iNos*, inducible nitric oxide synthase; KEAP1, Kelch-like ECH-associated protein 1; KO, knockout; MDA, malondialdehyde; NaB, sodium butyrate; NG, normal glucose; n-NRF2, nuclear NRF2; NQO1, NAD(P)H dehydrogenase quinone 1; NRF2, nuclear factor erythroid 2-related factor 2; PE, phenylephrine; ROS, reactive oxygen species; SFN, sulforaphane; STZ, streptozotocin; t-NRF2, total cellular NRF2; VCAM-1, vascular cell adhesion molecule-1; WT, wild type

Keywords: aorta; diabetes; endothelial dysfunction; inflammation; oxidative stress

1. Introduction

Over a half of the diabetic individuals develop macrovascular complications [1, 2]. Since the prevalence of diabetes mellitus (DM) has been dramatically increasing in recent years [3, 4], it is urgently needed to develop novel effective medicines to prevent or slowdown the progression of diabetic macrovascular complications.

Endothelial dysfunction is the critical first step to the development of diabetic vascular complications, with increased oxidative stress and inflammation as major contributors [5-9]. Within the vicious circle between oxidative stress and inflammation in atherogenesis [7], oxidative stress directly generates pro-inflammatory and adhesion molecules, and facilitates leukocyte or monocyte infiltration [6, 8]. Thus, targeting oxidative stress is an effective strategy to attenuate DM-induced endothelial injury.

One approach to block DM-induced oxidative stress is the nuclear factor erythroid 2-related factor 2 (NRF2) antioxidant signaling pathway. NRF2 is a master regulator of cellular antioxidant activity [10, 11] and activates the transcription of various antioxidant genes, such as NAD(P)H dehydrogenase quinone 1 (*Nqo1*) and heme oxygenase 1 (*Ho1*) [12], thereby producing antioxidants that act as scavengers for DM-induced free radicals. In the cytoplasm, NRF2 is sequestered by Kelch-like ECH-associated protein 1 (KEAP1), which restricts NRF2 from nuclear translocation and induces NRF2 proteasomal degradation [13]. NRF2 plays an essential role in self-defense against diabetic cardiomyopathy [14, 15] and nephropathy [16-18], since *Nrf2* gene knockout (KO) mice develop more severe DM-induced heart [14, 15] and kidney injury [16-18], as compared with wild type (WT) mice. Previous reports highlighted the

beneficial effects of NRF2 activation by small molecule inhibitors of KEAP1, including sulforaphane (SFN) [19], dh404 [5] and dimethyl fumarate [20], on DM-induced aortic injury. However, it was still unclear whether or to what extent NRF2 was required for self-protection and the actions of these NRF2 activators in the diabetic aorta. Thus, the use of *Nrf2* KO mice should be helpful to elucidate the role of NRF2 in these regards.

Sodium butyrate (NaB) is a fatty acid derivative found in human diet, such as parmesan cheese and butter, and is also produced in large amounts from fermentation of dietary fiber in the large intestine [21]. NaB was primarily known as an histone deacetylase (HDAC) inhibitor [22]. Not until recent years was NaB found to be an activator of NRF2 [23]. However, little was known for the mechanism by which NaB activates NRF2. Additionally, the effect of NaB on DM-induced aortic oxidative stress and inflammation has not been studied and reported. We previously reported the protection of NaB against diabetic nephropathy [24], which is a microvascular complication of DM. NaB induced renal *Nrf2* gene transcription and translation without facilitating NRF2 nuclear translocation [24]. Specifically, NaB increased the amount of *Nrf2* mRNA, total cellular NRF2 protein (t-NRF2), cytosolic NRF2 protein (c-NRF2) and nuclear NRF2 protein (n-NRF2), but not the proportion of n-NRF2 out of t-NRF2 [24]. These findings suggest a NRF2-regulating mechanism of NaB distinct from that of the small molecule inhibitors of KEAP1. However, the mechanism of NaB in activating *Nrf2* gene transcription remained unclear.

Histone modifications modulate the packing of chromatin, which determines the access of the transcriptional machinery to the promoter in order for transcription to occur [25]. HDAC encourages high-affinity binding between the histones and DNA backbone, the effect of which condenses DNA structure, thereby preventing gene transcription [26]. In contrast, histone

acetylase, such as P300, reduces affinity between histones and DNA, facilitating transcription factor binding to gene promoters [25]. We therefore propose that NaB inhibits HDAC activity, facilitating recruitment of the known *Nrf2*'s transcription factor aryl hydrocarbon receptor (AHR) [27] and the co-activator P300 to the promoter of the *Nrf2* gene, followed by its transcription.

Collectively, the present study aimed to research the effect of NaB on DM-induced aortic endothelial dysfunction. To test whether or to what extent NRF2 is required for both self-defense and NaB's protection, C57BL/6 WT and *Nrf2* KO mice were induced to DM by streptozotocin (STZ), and were treated in the presence or absence of NaB, for 20 weeks. To confirm the level at which NaB regulates aortic endothelial *Nrf2* expression, *Nrf2* mRNA and NRF2 nuclear translocation were determined in NaB- or SFN-treated, high glucose (HG)-cultured aortic endothelial cells (ECs). In order to further explore the mechanism through which NaB activates *Nrf2* gene transcription, HDAC activity and AHR and P300 occupancy at the *Nrf2* promoter were measured. Finally, the requirement of P300 in mediating NaB's activation of *Nrf2* expression and function was tested using the P300 inhibitor C646 [28].

2. Materials and methods

2.1 Animal housing

C57BL/6 WT (*Nrf2*^{+/+}) and *Nrf2* KO (*Nrf2*^{-/-}) mice were obtained through breeding of heterozygotes (*Nrf2*^{+/-}) [11, 24, 29]. All the mice were housed in the Animal Center of Jilin University at 22°C, on a 12:12-h light-dark cycle with free access to rodent feed and tap water. The Institutional Animal Care and Use Committee at Jilin University approved all experimental procedures for the animals. Consequently, this procedure was in accordance with the

International Guiding Principles for Biomedical Research Involving Animals, as issued by the Council for the International Organizations of Medical Sciences.

2.2 Animal treatment

Eight-week-old male mice received either sodium citrate or STZ (50 mg/kg daily, dissolved in 0.1 M sodium citrate, pH 4.5; Sigma-Aldrich, Shanghai, PRC) through intraperitoneal injection for 5 consecutive days [11, 18, 30]. Fasting glucose levels (4-hour fast) were measured a week after the last injection of STZ. Mice with a fasting glucose level above 13.89 mM were considered diabetic. The diabetic and age-matched control (Ctrl) mice were then given either a 5% NaB (PureOne Biotechnology, Shanghai, PRC) diet or a standard diet, as described previously [24, 31]. Consequently, the mice received a NaB diet at ~ 5g/kg/day [24, 31] or a standard diet, at the normal daily rate of caloric intake, for a total period of 20 weeks. Blood glucose levels were recorded on days 0, 28, 56, 84, 112 and 140 post DM onset. At the end of the procedures, all the mice were euthanized under anaesthesia by an intraperitoneal injection of chloral hydrate at 0.3 mg/kg [32] and their aortas were harvested for analysis.

2.3 Vascular reactivity

Enhanced vascular contractility and impaired vascular relaxation are two key features of diabetic endothelial dysfunction [5]. Thus, vascular contractility and relaxation were evaluated by measuring the contraction in response to phenylephrine (PE) and relaxation in response to acetylcholine (ACh), using the thoracic aortas. The thoracic aortas were cut into 4 mm segments and mounted on two L-shaped metal prongs. One prong was linked to a force-displacement transducer for continuous recording of isometric tension and the other was connected to a

displacement device which allowed adjustment of the distance between the two parallel prongs. The thoracic aortas were equilibrated for 45 minutes and normalized at 0, 15 and 25 mN to obtain the final micrometer setting between the prongs [5]. The thoracic aortas were then subjected to an oxygenated and pre-warmed high potassium physiological salt solution (KPSS, at 37 °C), containing KCl 123 mM, MgSO₄·7H₂O 1.17 mM, NaHCO₃ 25 mM, KH₂PO₄ 1.18 mM, CaCl₂ 2.5 mM, glucose 6.05 mM and EDTA 0.03 mM [5], to determine the viability of the aortas. Vascular reactivity in response to PE and ACh (both at 10⁻⁹, 10⁻⁸, 10⁻⁷, 10⁻⁶, 10⁻⁵ and 10⁻⁴ M) was recorded.

2.4 Histology

The freshly harvested thoracic aortas were fixed immediately into 10% buffered formalin solution and were embedded in paraffin, followed by sectioning into 5- μ m-thick sections onto glass slides. Hematoxylin and eosin staining was performed to evaluate the morphological change. Selection of areas to photograph and scoring was done by people blind to the identity of the samples.

2.5 Immunohistochemical (IHC) staining

The procedure of IHC staining was as previously described [33], using antibodies against 3-nitrotyrosine (3-NT, Millipore, Temecula, CA, USA; 1:100), 4-hydroxynonenal (4-HNE, Alpha Diagnostic Int., San Antonio, TX, USA; 1:100), HO1 (Cell Signaling Technology; Danvers, MA, USA; 1:100), intercellular adhesion molecule-1 (ICAM-1, Santa Cruz Biotechnology, Dallas, TX, USA; 1:100), NRF2 (Santa Cruz Biotechnology; 1:100) and vascular cell adhesion molecule-1

(VCAM-1, Santa Cruz Biotechnology; 1:100). Selection of areas to photograph and scoring was done by people blind to the identity of the samples.

2.6 Cell culture and experiments

ECs were isolated from the aortas of 8-week-old C57BL/6 WT male mice, following the established protocol for aortic EC isolation in mouse [34]. Briefly, each mouse was anesthetized by an intraperitoneal injection of chloral hydrate at 0.3 mg/kg [32]. The abdominal aorta was exposed and cut at the middle to release the blood. The aorta was perfused from the left ventricle, with PBS containing 1000 U/ml heparin, dissected out from the aortic arch to the abdominal aorta, and then immersed in 20% fetal bovine serum (FBS; Gibco, Shanghai, PRC)-normal glucose (NG; 1 g/L) Dulbecco's Modified Eagle Medium (DMEM; Gibco) containing 1000 U/ml heparin. The fat and connecting tissue were quickly removed under a stereoscopic microscope. The inside of the lumen was washed with serum-free DMEM (NG), filled with collagenase II (2 mg/ml), and incubated at 37 °C, for 45 minutes. ECs were removed by flushing with 5 ml 20% FBS-DMEM (NG), and collected by centrifuging at 1200 rpm, for 5 minutes. The cells were then suspended gently by pipette with 20% FBS-DMEM (NG), and seeded in a collagen I-coated dish. After 7 to 10 days, confluent ECs were observable. After 2-3 passages, ECs were maintained in 10% FBS-DMEM (NG).

To test NaB's protection in ECs, ECs were treated with NG, NG/mannitol (3.64 g/L), HG (4.5 g/L), or HG/NaB respectively, for 48 hours. To verify the role of NRF2 in NaB's action, ECs were treated with HG in combination with NaB (PureOne Biotechnology) at 1 mM [35-37], in the presence of either *Nrf2* siRNA (20 nM [38], GenePharma, Suzhou, Jiangsu, PRC) or its negative control (GenePharma). The transfection reagent Rfect^{PM} was provided by Changzhou

Bio-generating Biotechnologies (Changzhou, Jiangsu, PRC). With the aim of verifying the exact level at which NaB activates *Nrf2*, HG-treated ECs were co-treated with either NaB or SFN (10 μ M [39-41], Sigma-Aldrich), for 48 hours. In order to further explore the mechanism by which NaB activates *Nrf2*, HG-treated ECs were subjected to NaB, in the presence or absence of C646 (25 μ M [28], MedChem Express, Shanghai, PRC), for 48 hours.

2.7 Isolation of nuclei

Nuclei of ECs were isolated using a nuclei isolation kit (Sigma-Aldrich), following the manufacturer's instructions. Briefly, cells were gently washed with 10 ml ice cold PBS, followed by 10 ml iced cold Lysis Solution containing DTT and Triton X-100 added to each dish. The cells were then harvested and lysed by scraping with a bladed cell scraper. Cell lysate from all dishes was transferred into a 15 ml centrifuge tube, mixed with 1.8 M Sucrose Cushion Solution and centrifuged at 4 °C at 30,000 g, for 45 minutes. The nuclei were visible as a small, thin pellet at the bottom of the tube. The supernatant was saved for analysis of cytosolic NRF2. The nuclei pellet was further processed and stored with Nuclei PURE Storage Buffer.

2.8 HDAC activity assay

HDAC activity was determined using a HDAC assay kit (BioVision, Milpitas, CA, USA) following the manufacturer's protocol. Briefly, 25 μ g of cell lysate was diluted to 85 μ l of ddH₂O in each well. 10 μ l of the 10 \times HDAC Assay Buffer and 5 μ l of the HDAC Fluorometric Substrate were added to each well. After mixing thoroughly, plates were incubated at 37 °C for 30 minutes. Reaction was then terminated by adding 10 μ l of Lysine Developer, incubating for

30 minutes. Fluorescence signal was detected with the excitation at 360 nm and emission at 460 nm, using a fluorescence microplate reader (BioTek, Winooski, VT, USA).

2.9 Chromatin immunoprecipitation (ChIP) assay

ChIP assay was performed, with ChIP-enriched DNA analyzed by real-time PCR (RT-PCR). Briefly, ECs were fixed with 1% formaldehyde at 37 °C for 10 minutes, washed with cold PBS containing protease inhibitors, and lysed in Tris (pH 8.1) containing 1% SDS, 1 mM PMSF, and complete protease inhibitor cocktail. Cell lysates were sonicated to fragment chromatin into 500-bp size, diluted in ChIP dilution buffer, and immunoprecipitated overnight at 4 °C with antibodies against AHR (Abcam, Shanghai, PRC) and P300 (Santa Cruz Biotechnology). The immune complexes were then collected on protein-A agarose beads, which were washed to remove nonspecific binding. DNA was eluted from the beads, with cross-links reversed and DNA extracted. ChIP-enriched DNA samples were analyzed by RT-PCR, using primers specific for the *Nrf2* promoter (GenePharma).

2.10 Quantitative analysis of reactive oxygen species (ROS) and lipid peroxides

ROS and malondialdehyde (MDA) levels were measured in cell lysates, by using a ROS assay kit (Nanjing Jiancheng Bioengineering Institute, Nanjing, Jiangsu, PRC) and a lipid peroxidation assay kit (Sigma-Aldrich) respectively, following the manufacturers' instructions.

2.11 Quantitative real-time PCR (qPCR)

Thoracic aortas and cell lysates were used for qPCR (TaqMan), as previously described [33]. The primers for glyceraldehyde 3-phosphate dehydrogenase (*Gapdh*, ID: Mm99999915_g1), *Ho-*

I (ID: Mm00516005_m1), *Icam-1* (ID: Mm00516023_m1), inducible nitric oxide synthase (*iNos*, ID: Mm00440502_m1), *Nqo1* (ID: Mm01253561_m1), *Nrf2* (ID: Mm00477784_m1) and *Vcam-1* (ID: Mm01320970_m1) were all purchased from Life technologies (Shanghai, PRC).

2.12 Western blot

Western blot analysis was performed using cell lysates, as described in our previous studies [33, 42]. Briefly, proteins were collected from cell lysates, by centrifuging at 12,000 g at 4 °C for 15 min, with concentration measured using Bradford assay. After diluting in loading buffer and heating at 95 °C for 5 minutes, the samples were subjected to electrophoresis on SDS-PAGE gel at 120 V. After electrophoresis, the proteins were transferred to nitrocellulose membranes, blocked in blocking buffer (5% milk and 0.5% BSA) for 1 hour, and washed 3 times with Tris-buffered saline containing 0.05% Tween 20 (Beyotime Biotechnology, Shanghai, PRC). The membranes were incubated with primary antibodies overnight, washed as aforementioned and reacted with secondary horseradish peroxidase-conjugated antibodies at room temperature for 1 hour. The primary antibodies used were anti-3-NT (Millipore, 1:1000), anti-4-HNE (Alpha Diagnostic Int., 1:1000), anti-GAPDH (Santa Cruz Biotechnology, 1:3000), anti-histone H3 (Santa Cruz Biotechnology, 1:1000), anti-ICAM-1 (Santa Cruz Biotechnology; 1:500), anti-HO1 (Cell signaling Technology; 1:1000), anti-NRF2 (Santa Cruz Biotechnology, 1:1000), anti-VCAM-1 (Santa Cruz Biotechnology, 1:1000).

2.13 Statistical analysis

Seven mice per group were studied. Cell experiments were performed in triplicate. The measurements for each group were summarized as means \pm SD. Western blots were analyzed by

Image Quant 5.2 software (GE Healthcare Bio-Sciences, Pittsburgh, PA, USA). IHC positive area was quantified using Image Pro Plus 6.0 software (Media Cybernetics, Rockville, MD, USA). One-way ANOVA, two-way ANOVA and Student's *t*-test were performed for the comparisons, using Origin 8.6 data analysis and graphing software Lab (OriginLab, Northampton, MA, USA). A test is significant if $p < 0.05$.

3. Results

3.1 NaB improved DM-induced aortic endothelial dysfunction in the WT, but not the *Nrf2* KO, mice.

Blood glucose levels were monitored in all the mice every four weeks post DM onset (Fig. 1A). Significantly increased blood glucose levels were observed in the STZ-treated mice, but not the Ctrl mice (Fig. 1A). Neither *Nrf2* gene deletion nor NaB treatment altered blood glucose levels in the diabetic mice (Fig. 1A). Thus, the impact of NaB on the DM-induced aortic injury, if any, must not be owing to the attenuation of hyperglycemia. To assess the role of NRF2 in NaB's effect on diabetes-induced vascular dysfunction, aortic contractility and relaxation in response to either PE or ACh were determined in both the WT and the *Nrf2* KO mice, in the presence or absence of NaB (Fig. 1B, C). The aortas of both the WT and the *Nrf2* KO diabetic mice had a significantly enhanced contraction in response to PE at the doses from 10^{-8} M to 10^{-4} M, as compared with their respective Ctrl mice (Fig. 1B). The contraction of the diabetic aortas exhibited more prominently in response to 10^{-7} , 10^{-6} , 10^{-5} and 10^{-4} M PE in the *Nrf2* KO mice, as compared with that in the WT mice (Fig. 1B). NaB diminished the aortic contractility in response to 10^{-8} , 10^{-7} , 10^{-6} , 10^{-5} and 10^{-4} M PE in the WT, but not the *Nrf2* KO, mice (Fig. 1B). In the presence of ACh at the doses of 10^{-8} , 10^{-7} , 10^{-6} , 10^{-5} and 10^{-4} M, the NaB-treated diabetic aortas

were rescued from the DM-impaired relaxation in the WT, but not the *Nrf2* KO, mice (Fig. 1C). H&E staining (Fig. 1D) revealed a slight increase in tunica media induced by DM [43, 44], which was prevented by NaB in the WT, rather than the *Nrf2* KO, mice (Fig. 1C).

Accepted manuscript

Fig. 1

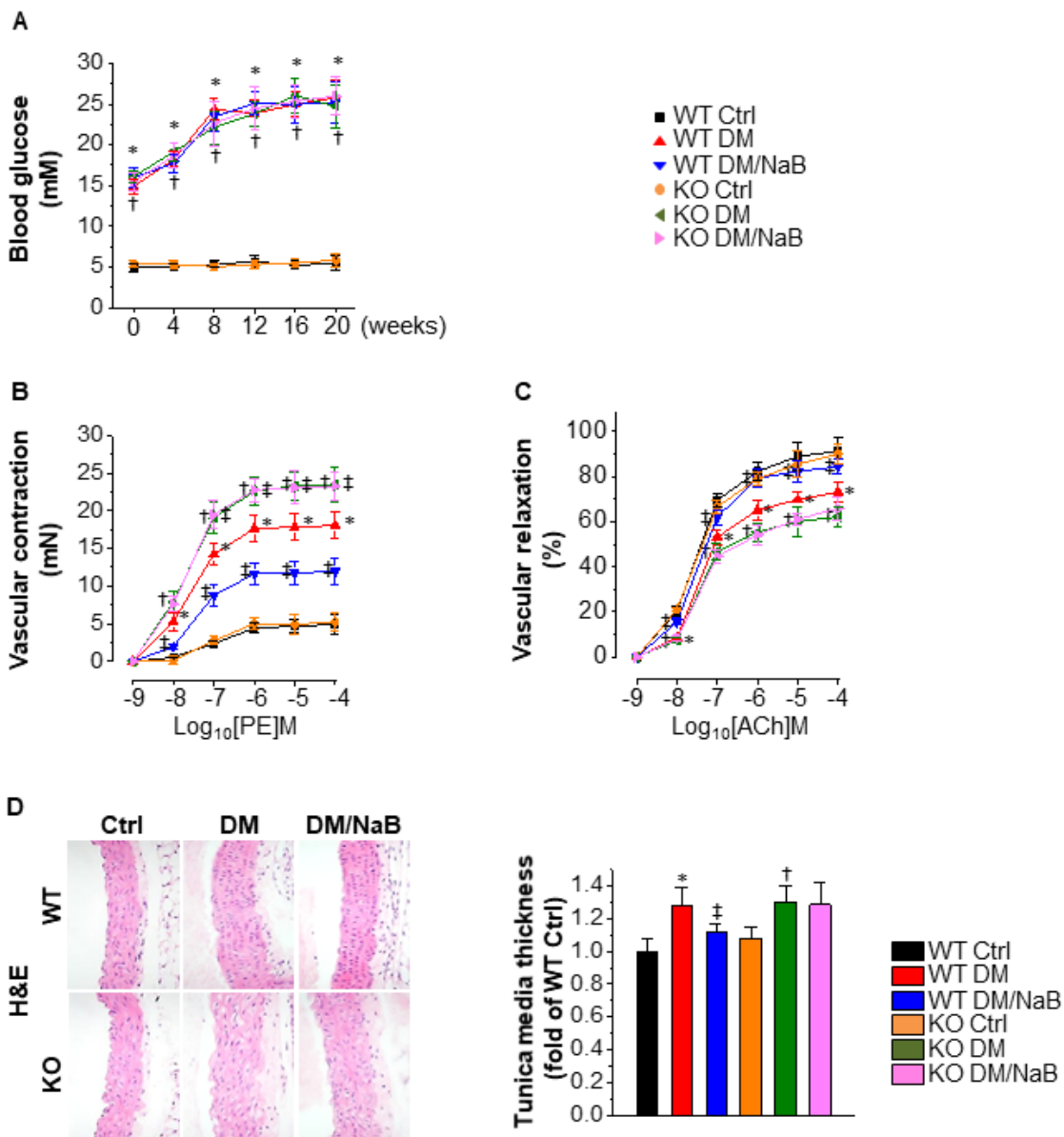


Fig. 1. NaB prevented DM-enhanced aortic contractility in the WT, but not the *Nrf2* KO, mice. Eight-week-old C57BL/6 WT and *Nrf2* KO male mice were induced to DM by STZ. (A) Blood glucose levels were recorded at 0, 4, 8, 12, 16 and 20 weeks post DM onset. (B) Vascular contractility was assessed by determining aortic contraction in response to PE at doses of 10^{-9} , 10^{-8} , 10^{-7} , 10^{-6} , 10^{-5} and 10^{-4} M. (C) Vascular relaxation in the presence of ACh at 10^{-9} , 10^{-8} , 10^{-7} , 10^{-6} , 10^{-5} and 10^{-4} M were measured. (D) H&E staining was performed for morphological analysis, with the thickness of tunica media measured. For (D), the data was normalized to WT Ctrl. All the data is presented as means \pm SD ($n = 7$). *, $p < 0.05$ vs WT Ctrl; †, $p < 0.05$ vs KO Ctrl; ‡, $p < 0.05$ vs WT DM. Scatter plots and bars: black, WT Ctrl; red, WT DM; blue, WT DM/NaB; orange, KO Ctrl; green, KO DM; pink, KO DM/NaB. Abbreviations: ACh, acetylcholine; Ctrl, control; DM, diabetes mellitus; H&E, hematoxylin and eosin; KO, knockout; NaB, sodium butyrate; PE, phenylephrine; STZ, streptozotocin; WT, wild type.

Fig. 1. NaB prevented DM-enhanced aortic contractility in the WT, but not the *Nrf2* KO, mice. Eight-week-old C57BL/6 WT and *Nrf2* KO male mice were induced to DM by STZ. (A) Blood glucose levels were recorded at 0, 4, 8, 12, 16 and 20 weeks post DM onset. (B) Vascular contractility was assessed by determining aortic contraction in response to PE at doses of 10^{-9} , 10^{-8} , 10^{-7} , 10^{-6} , 10^{-5} and 10^{-4} M. (C) Vascular relaxation in the presence of ACh at 10^{-9} , 10^{-8} , 10^{-7} , 10^{-6} , 10^{-5} and 10^{-4} M were measured. (D) H&E staining was performed for morphological analysis, with the thickness of tunica media measured. For (D), the data was normalized to WT Ctrl. All the data is presented as means \pm SD (n = 7). *, $p < 0.05$ vs WT Ctrl; †, $p < 0.05$ vs KO Ctrl; ‡, $p < 0.05$ vs WT DM. Scatter plots and bars: black, WT Ctrl; red, WT DM; blue, WT DM/NaB; orange, KO Ctrl; green, KO DM; pink, KO DM/NaB. Abbreviations: ACh, acetylcholine; Ctrl, control; DM, diabetes mellitus; H&E, hematoxylin and eosin; KO, knockout; NaB, sodium butyrate; PE, phenylephrine; STZ, streptozotocin; WT, wild type.

3.2 NRF2 was required for NaB's protection against DM-induced aortic oxidative stress and inflammation.

To test the effect of NaB on DM-induced aortic oxidative stress and inflammation, indicators for oxidative damage and inflammation were evaluated by IHC staining and RT-PCR. In the aortas of the WT mice, hyperglycemia enhanced endothelial protein expression of 3-NT (Fig. 2A), 4-HNE (Fig. 2B), VCAM-1 (Fig. 2C) and ICAM-1 (Fig. 2D), as well as the mRNA expression of *iNos* (Fig. 2E) and *Vcam-1* (Fig. 2F), the effects of which were significantly prevented by NaB (Fig. 2A-F). These protective effects of NaB were not observed in the aortas of the *Nrf2* KO mice (Fig. 2A-F). Therefore, these results demonstrate that NRF2 predominantly mediates NaB's protection against DM-induced aortic oxidative stress and inflammation. Notably, the *Nrf2* KO diabetic mice developed more severe aortic oxidative stress and inflammation, as compared with the WT diabetic mice (Fig. 2A-F), establishing the essential role of NRF2 in self-protection against DM-induced aortic injury.

Fig. 2

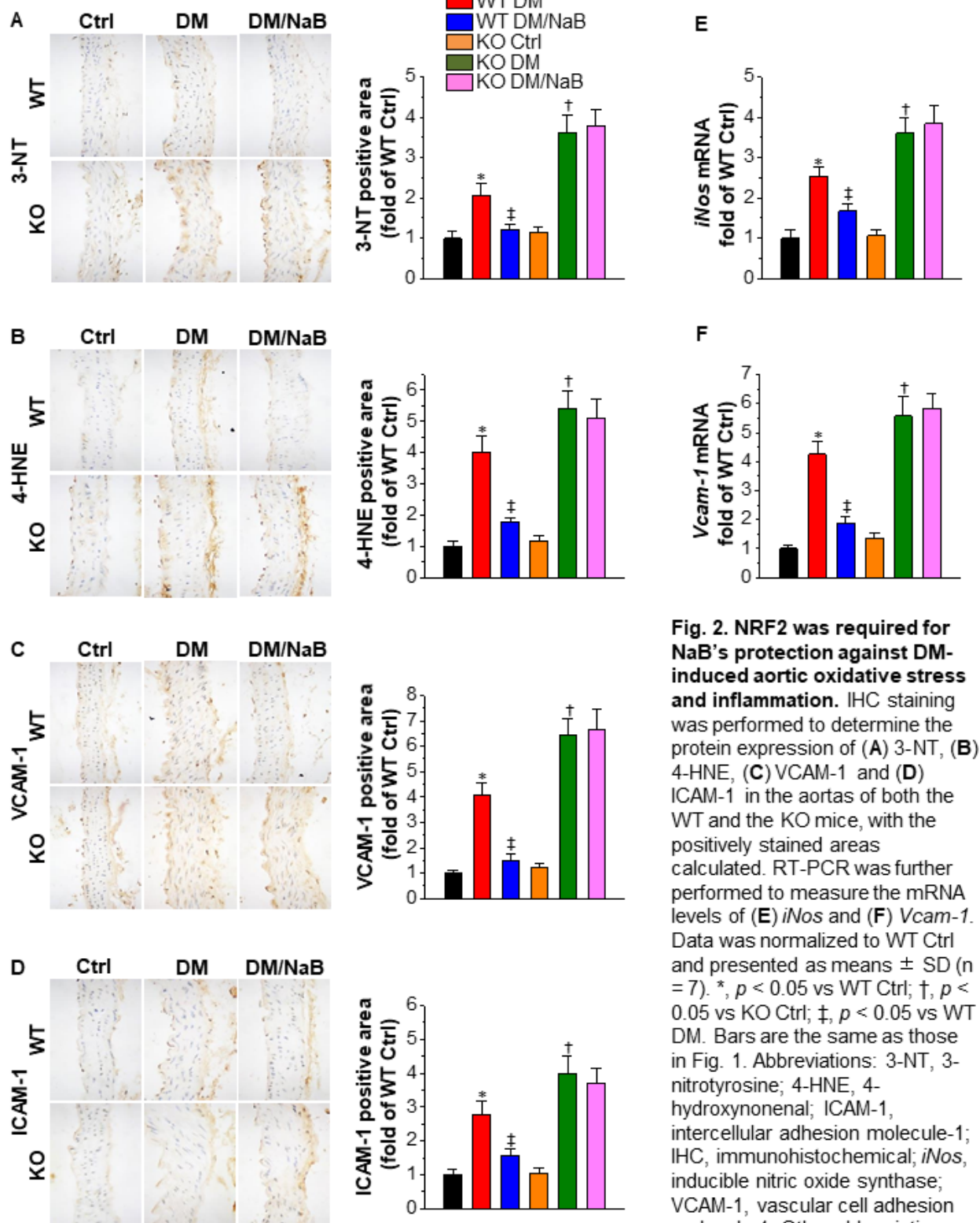


Fig. 2. NRF2 was required for NaB's protection against DM-induced aortic oxidative stress and inflammation. IHC staining was performed to determine the protein expression of (A) 3-NT, (B) 4-HNE, (C) VCAM-1 and (D) ICAM-1 in the aortas of both the WT and the KO mice, with the positively stained areas calculated. RT-PCR was further performed to measure the mRNA levels of (E) *iNos* and (F) *Vcam-1*. Data was normalized to WT Ctrl and presented as means \pm SD (n = 7). *, $p < 0.05$ vs WT Ctrl; †, $p < 0.05$ vs KO Ctrl; ‡, $p < 0.05$ vs WT DM. Bars are the same as those in Fig. 1. Abbreviations: 3-NT, 3-nitrotyrosine; 4-HNE, 4-hydroxynonenal; ICAM-1, intercellular adhesion molecule-1; IHC, immunohistochemical; *iNos*, inducible nitric oxide synthase; VCAM-1, vascular cell adhesion molecule-1. Other abbreviations are the same as in Fig. 1.

3.3 NaB activated *Nrf2* expression and function in the aortas of the WT diabetic mice

Given that NRF2 was required for NaB's prevention of DM-induced aortic injury (Fig. 2A-F), the effect of NaB on aortic *Nrf2* expression and function was evaluated. NaB increased both *Nrf2* mRNA (Fig. 3A) and protein (Fig. 3B) levels, so did it enhance *Ho1* mRNA (Fig. 3C) and protein (Fig. 3D) levels, in the aortas of the WT diabetic mice. *Nrf2* mRNA (Fig. 3A) and protein (Fig. 3B) were not detectable in the aortas of the *Nrf2* KO mice, as a confirmation of the *Nrf2* gene deletion. The *Nrf2* KO mice had much less aortic expression of *Ho1*, as compared with the WT mice (Fig. 3C, D). NaB failed to enhance *Ho1* expression in the absence of NRF2 (Fig. 3C, D). Therefore, NRF2 was found to be a key factor that controls aortic antioxidant activity, and mediates NaB's antioxidative effect in the diabetic aorta.

Fig. 3

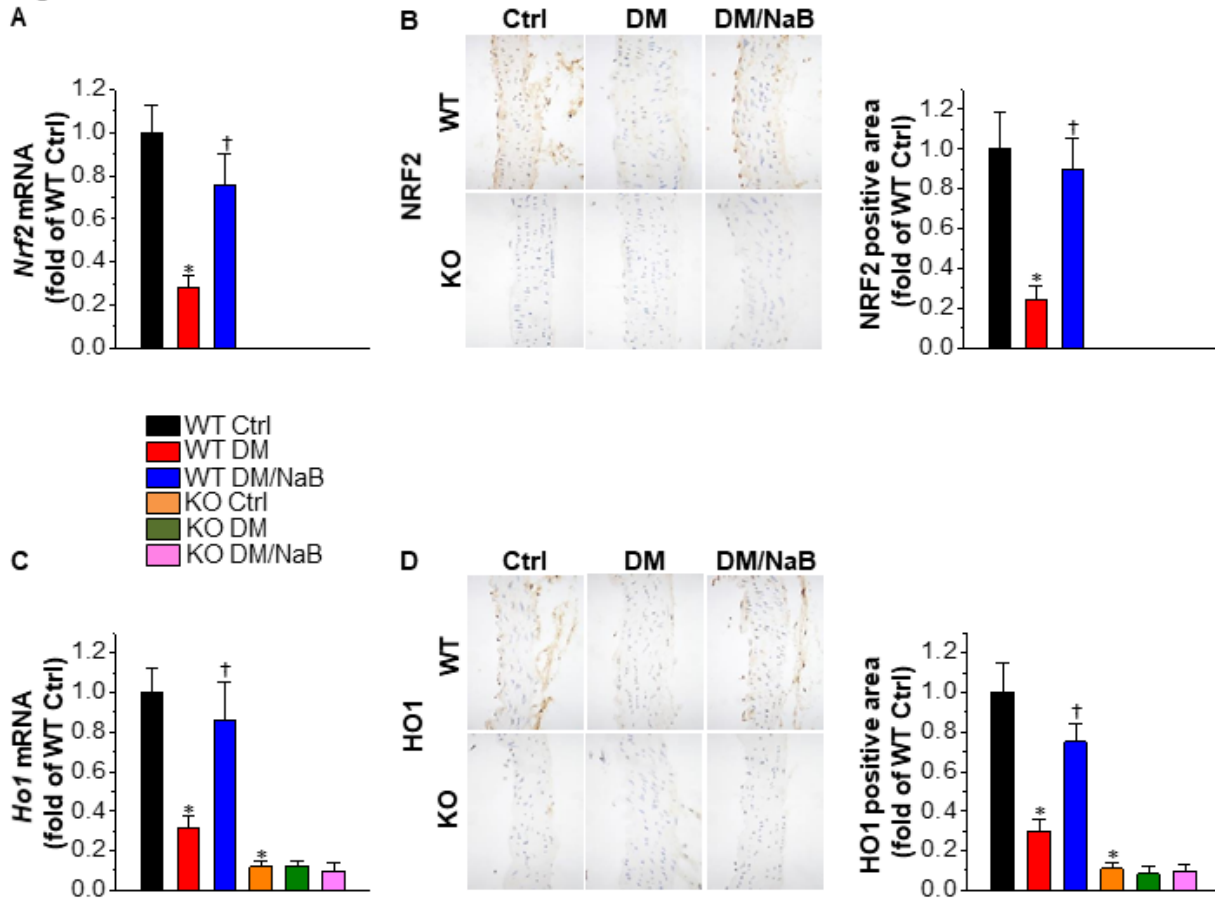


Fig. 3. NaB activated *Nrf2* expression and function in the aortas of the WT diabetic mice. *Nrf2* (A) mRNA and (B) protein, as well as *Ho1* (C) mRNA and (D) protein were determined in both the WT and the KO mice by RT-PCR and IHC staining respectively, with the IHC positive areas quantified. Data was normalized to WT Ctrl and presented as means \pm SD ($n = 7$). *, $p < 0.05$ vs WT Ctrl; †, $p < 0.05$ vs WT DM. Bars are the same as those in Fig. 1. Abbreviations: NRF2, Nuclear factor erythroid 2-related factor 2; HO1, heme oxygenase 1. Other abbreviations are the same as in Fig. 1.

Fig. 3. NaB activated *Nrf2* expression and function in the aortas of the WT diabetic mice. *Nrf2* (A) mRNA and (B) protein, as well as *Ho1* (C) mRNA and (D) protein were determined in both the WT and the KO mice by RT-PCR and IHC staining respectively, with the IHC positive areas quantified. Data was normalized to WT Ctrl and presented as means \pm SD (n = 7). *, $p < 0.05$ vs WT Ctrl; †, $p < 0.05$ vs WT DM. Bars are the same as those in Fig. 1. Abbreviations: NRF2, Nuclear factor erythroid 2-related factor 2; HO1, heme oxygenase 1. Other abbreviations are the same as in Fig. 1.

3.4 NRF2 predominantly mediated NaB's effect on the attenuation of HG-induced aortic endothelial oxidative stress and inflammation.

Endothelium is directly exposed to serum stimuli, such as high blood glucose. In the present study, hyperglycemia-induced aortic oxidative stress and inflammation were found to be abundantly located in the endothelium (Fig. 2A-D). In contrast, NRF2 and NQO1 were highly expressed in the endothelium of the WT Ctrl mice, and were less expressed under the diabetic condition, the effect of which was reversed by NaB (Fig. 3B, D). These results indicate the active involvement of EC in hyperglycemia-induced aortic injury. Therefore, EC was culled for the tests in the following studies.

In order to test the impact of HG on endothelial NRF2 signaling and injury, ECs were treated with either NG or HG. To verify the role of NRF2 in mediating NaB's protective effect on HG-induced endothelial injury, ECs were treated with HG and NaB, in the presence or absence of *Nrf2* siRNA. As shown in Fig. 4A-D, HG resulted in a significant reduction of *Nrf2* expression (Fig. 4A, B) and the transcription of *Nqo1* (Fig. 4C) and *Ho1* (Fig. 4D), the effects of which were reversed by NaB (Fig. 4A-D). NaB markedly blunted the HG-enhanced ROS (Fig. 4E) and MDA (Fig. 4F), as well as mRNA expression of *Vcam-1* (Fig. 4G) and *Icam-1* (Fig. 4H). All these effects of NaB were abrogated by the *Nrf2* siRNA (Fig. 4A-H). Hence, in line with the observations *in vivo* (Fig. 2), NRF2 was found, in ECs, to be required for NaB's attenuation of HG-induced oxidative stress and inflammation.

Fig. 4

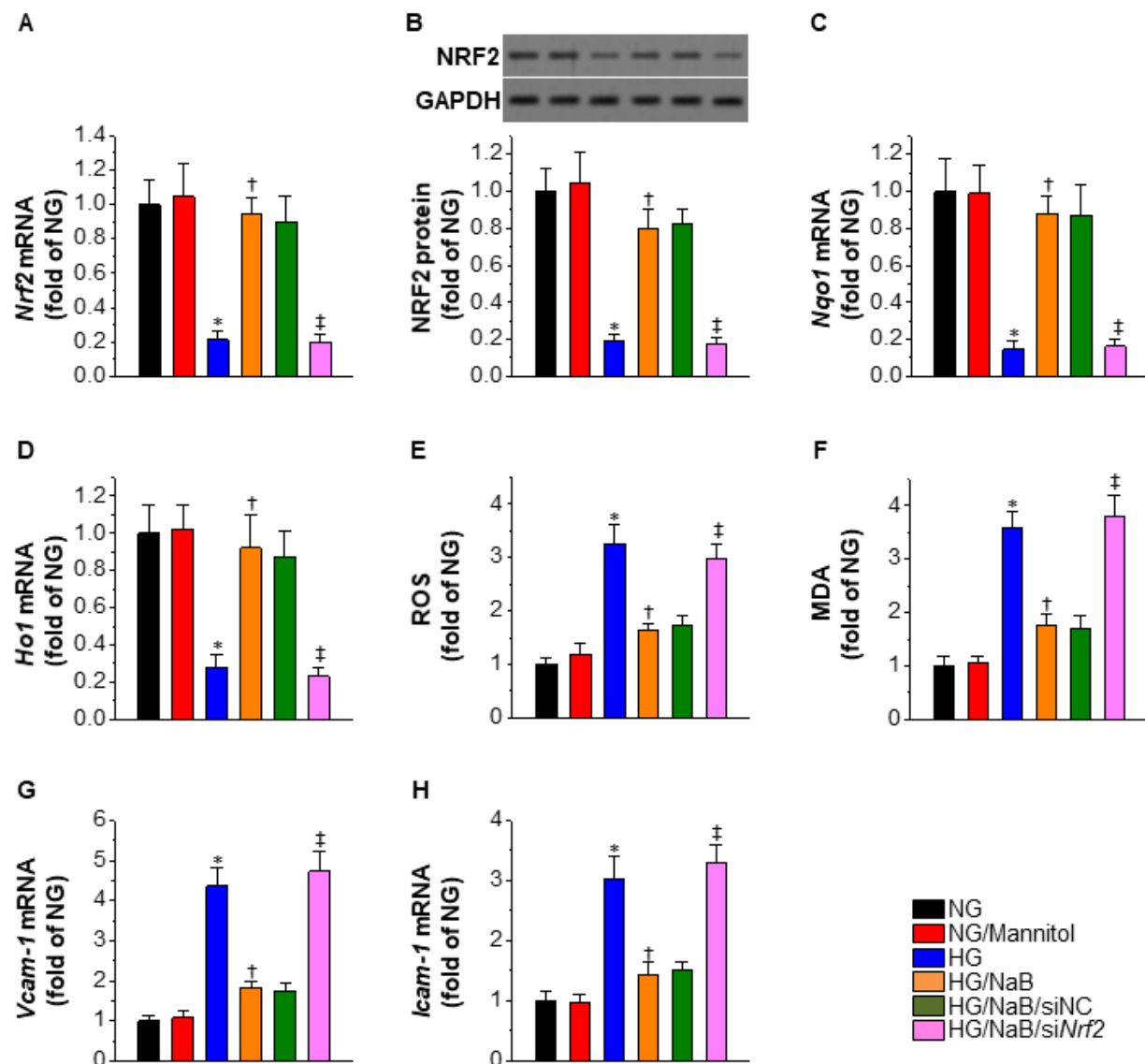


Fig. 4. NRF2 predominantly mediated NaB's effect on the attenuation of HG-induced aortic endothelial oxidative stress and inflammation. To test the role of NRF2 in NaB's protection against HG-induced aortic endothelial oxidative stress and inflammation, ECs were divided into the following groups: NG, NG/Mannitol, HG, HG/NaB, HG/NaB/siNC and HG/NaB/siNrf2. *Nrf2* (A) mRNA, (B) protein, and mRNA expression of (C) *Nqo1* and (D) *Ho1* were determined by RT-PCR and Western blot. In addition, levels of (E) ROS, (F) MDA were measured by assay kits and mRNA expression of (G) *Vcam-1* and (H) *Icam-1* determined by RT-PCR. Data was normalized to NG and presented as means \pm SD (n = 3). *, $p < 0.05$ vs NG; †, $p < 0.05$ vs HG. ††, $p < 0.05$ vs HG/NaB/siNC. Bars: white, NG; light grey, NG/Mannitol; dark grey, HG; black, HG/NaB; white with diagonal stripes, HG/NaB/siNC; light grey with diagonal stripes, HG/NaB/siNrf2. Abbreviations: HG, high glucose; *Ho1*, heme oxygenase 1; MDA, malondialdehyde; NG, normal glucose; ROS, reactive oxygen species; siNC, negative control siRNA; *siNrf2*, *Nrf2* siRNA. Other abbreviations are the same as in Figs. 1-3.

Fig. 4. NRF2 predominantly mediated NaB's effect on the attenuation of HG-induced aortic endothelial oxidative stress and inflammation. To test the role of NRF2 in NaB's protection against HG-induced aortic endothelial oxidative stress and inflammation, ECs were divided into the following groups: NG, NG/Mannitol, HG, HG/NaB, HG/NaB/siNC and HG/NaB/si*Nrf2*. *Nrf2* (A) mRNA, (B) protein, and mRNA expression of (C) *Nqo1* and (D) *Ho1* were determined by RT-PCR and Western blot. In addition, levels of (E) ROS, (F) MDA were measured by assay kits and mRNA expression of (G) *Vcam-1* and (H) *Icam-1* determined by RT-PCR. Data was normalized to NG and presented as means \pm SD (n = 3). *, $p < 0.05$ vs NG; †, $p < 0.05$ vs HG. ‡, $p < 0.05$ vs HG/NaB/siNC. Bars: white, NG; light grey, NG/Mannitol; dark grey, HG; black, HG/NaB; white with diagonal stripes, HG/NaB/siNC; light grey with diagonal stripes, HG/NaB/si*Nrf2*. Abbreviations: HG, high glucose; *Ho1*, heme oxygenase 1; MDA, malondialdehyde; NG, normal glucose; ROS, reactive oxygen species; siNC, negative control siRNA; si*Nrf2*, *Nrf2* siRNA. Other abbreviations are the same as in Figs. 1-3.

3.5 NaB activated *Nrf2* at the transcription level without facilitating NRF2 nuclear translocation.

To further explore the mechanism by which NaB activates NRF2, HG-treated ECs were co-treated with either NaB or SFN. Since SFN is known to inactivate KEAP1, thereby facilitating NRF2 nuclear translocation [13], the use of SFN might be helpful to understand the action of NaB. NaB, but not SFN, drastically increased *Nrf2* mRNA (Fig. 5A). Both NaB and SFN increased t-NRF2 (Fig. 5B) and c-NRF2 (Fig. 5C). However, NaB produced more t-NRF2 and c-NRF2, as compared with SFN (Fig. 5B, C). Interestingly, despite the less increased t-NRF2 and c-NRF2, SFN generated a similar level of n-NRF2 to that produced by NaB (Fig. 5D). We therefore speculated that SFN, but not NaB, triggers NRF2 nuclear translocation. We then calculated the ratio of n-NRF2/Histone H3 to c-NRF2/GAPDH (Fig. 5E), which could reflect NRF2 nuclear translocation. As expected, this ratio was significantly increased by SFN, but not NaB (Fig. 5E). Further, both NaB and SFN had similar effects on the induction of *Nqo1* (Fig. 5F) and *Ho1* (Fig. 5G) mRNAs. These results indicate that NaB activates *Nrf2* at the transcription level, without facilitating NRF2 nuclear translocation.

Fig. 5

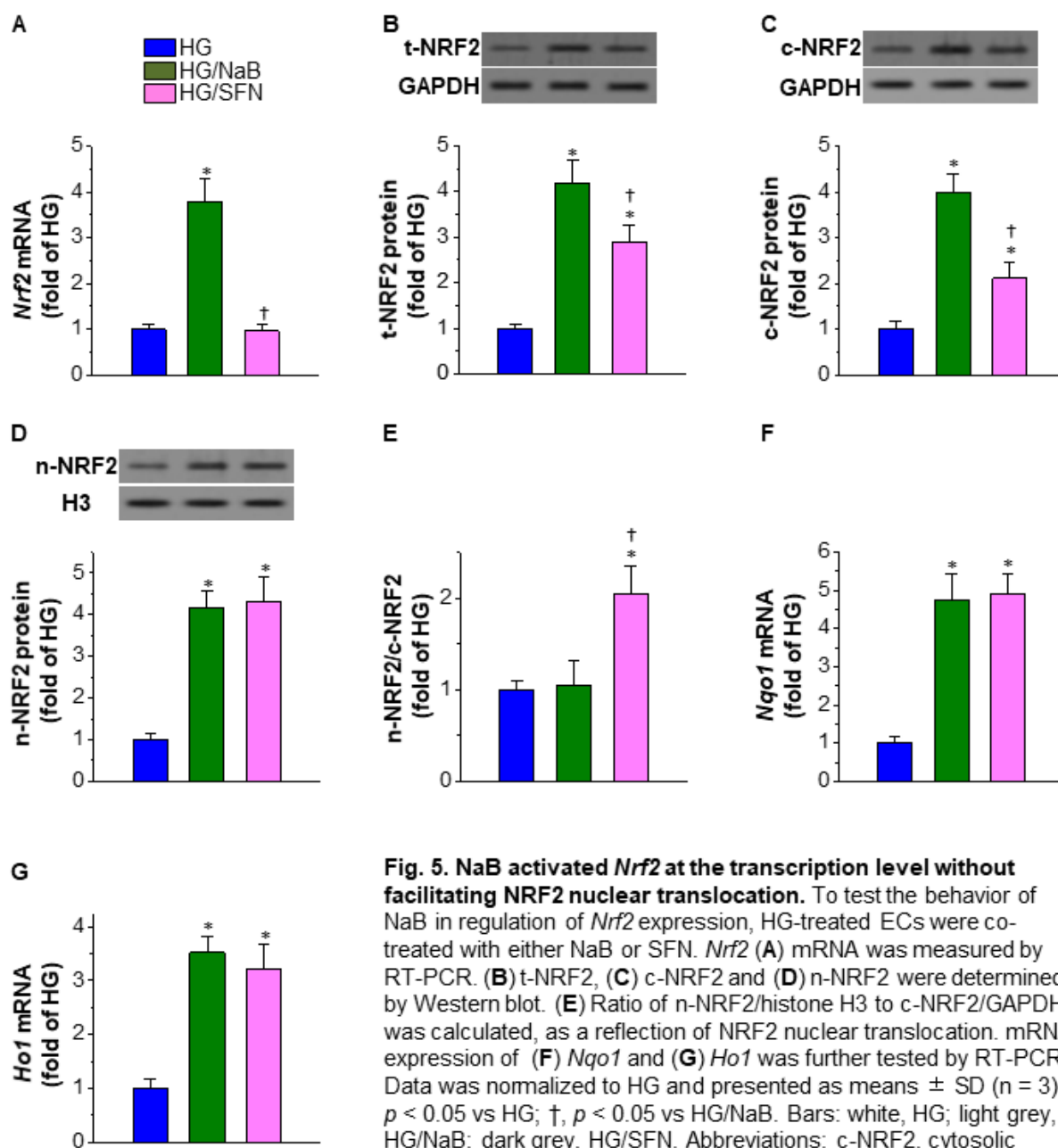


Fig. 5. NaB activated *Nrf2* at the transcription level without facilitating NRF2 nuclear translocation. To test the behavior of NaB in regulation of *Nrf2* expression, HG-treated ECs were co-treated with either NaB or SFN. *Nrf2* (A) mRNA was measured by RT-PCR. (B) t-NRF2, (C) c-NRF2 and (D) n-NRF2 were determined by Western blot. (E) Ratio of n-NRF2/histone H3 to c-NRF2/GAPDH was calculated, as a reflection of NRF2 nuclear translocation. mRNA expression of (F) *Nqo1* and (G) *Ho1* was further tested by RT-PCR. Data was normalized to HG and presented as means \pm SD (n = 3). *, $p < 0.05$ vs HG; †, $p < 0.05$ vs HG/NaB. Bars: white, HG; light grey, HG/NaB; dark grey, HG/SFN. Abbreviations: c-NRF2, cytosolic NRF2; n-NRF2, nuclear NRF2; SFN, sulforaphane; t-NRF2, total cellular NRF2. Other abbreviations are the same as in Figs. 1, 3, 4.

Fig. 5. NaB activated *Nrf2* at the transcription level without facilitating NRF2 nuclear translocation. To test the behavior of NaB in regulation of *Nrf2* expression, HG-treated ECs were co-treated with either NaB or SFN. *Nrf2* (A) mRNA was measured by RT-PCR. (B) t-NRF2, (C) c-NRF2 and (D) n-NRF2 were determined by Western blot. (E) Ratio of n-NRF2/histone H3 to c-NRF2/GAPDH was calculated, as a reflection of NRF2 nuclear translocation. mRNA expression of (F) *Nqo1* and (G) *Ho1* was further tested by RT-PCR. Data was normalized to HG and presented as means \pm SD (n = 3). *, $p < 0.05$ vs HG; †, $p < 0.05$ vs HG/NaB. Bars: white, HG; light grey, HG/NaB; dark grey, HG/SFN. Abbreviations: c-NRF2, cytosolic NRF2; n-NRF2, nuclear NRF2; SFN, sulforaphane; t-NRF2, total cellular NRF2. Other abbreviations are the same as in Figs. 1, 3, 4.

3.6 NaB inhibited HDAC activity and enhanced AHR and P300 binding at the promoter of the *Nrf2* gene in HG-treated ECs.

The following studies aimed to define the mechanism through which NaB activates *Nrf2* gene transcription. HG enhanced HDAC activity in ECs (Fig. 6A), the effect of which was markedly inhibited by NaB (Fig. 6A). Further, we determined the binding of AHR and P300 at the promoter region of the *Nrf2* gene by ChIP Assay. As expected, NaB increased the occupancy of both AHR and P300 at the promoter region of the *Nrf2* gene under the HG condition (Fig. 6B). These results indicate an important role of HDAC inhibition-induced chromatin structure change in regulation of *Nrf2* gene expression.

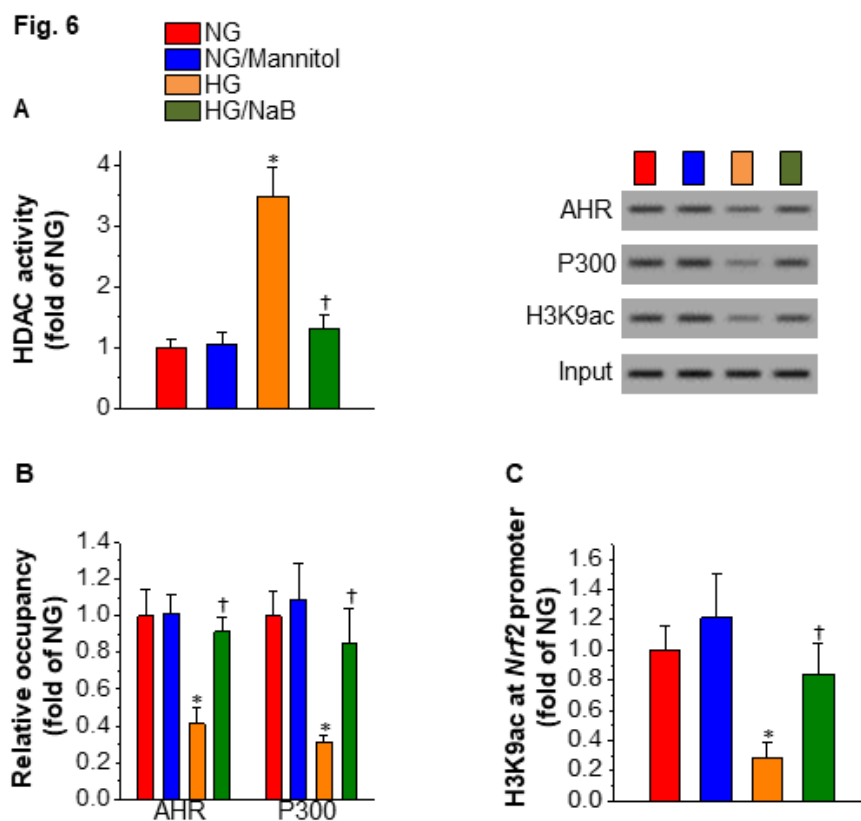


Fig. 6. NaB inhibited HDAC activity and enhanced AHR and P300 binding at the promoter of the *Nrf2* gene in HG-treated ECs. The effect of NaB on (A) HDAC activity was determined in NG or HG-treated ECs by an HDAC assay kit. Further, ChIP assay was performed to evaluate the occupancy of (B) AHR, P300 and (C) H3K9ac at the *Nrf2* gene promoter. Data was normalized to HG and presented as means \pm SD (n = 3). *, $p < 0.05$ vs HG. Bars: white, NG; light grey, NG/Mannitol; dark grey, HG; black, HG/NaB. Abbreviations: AHR, aryl hydrocarbon receptor; ChIP, chromatin immunoprecipitation; HDAC, histone deacetylase. Other abbreviations are the same as in Figs. 1, 4.

Fig. 6. NaB inhibited HDAC activity and enhanced AHR and P300 binding at the promoter of the *Nrf2* gene in HG-treated ECs. The effect of NaB on (A) HDAC activity was determined in NG or HG-treated ECs by an HDAC assay kit. Further, ChIP assay was performed to evaluate the occupancy of (B) AHR, P300 and (C) H3K9ac at the *Nrf2* gene promoter. Data was normalized to HG and presented as means \pm SD ($n = 3$). *, $p < 0.05$ vs HG. Bars: white, NG; light grey, NG/Mannitol; dark grey, HG; black, HG/NaB. Abbreviations: AHR, aryl hydrocarbon receptor; ChIP, chromatin immunoprecipitation; HDAC, histone deacetylase. Other abbreviations are the same as in Figs. 1, 4.

3.7 P300 mediated NaB-induced activation of *Nrf2* in HG-treated ECs.

Although NaB increased P300 binding at the *Nrf2* gene promoter (Fig. 6B, right panel), it was still unclear whether P300 plays a key role in mediating NaB-induced *Nrf2* gene transcription. Thus, ECs were treated with HG and NaB, in the presence or absence of the P300 selective inhibitor C646 [28]. C646 reversed the NaB-induced P300 and AHR binding at the promoter of the *Nrf2* gene (Fig. 7A), and abolished NaB-induced elevation of *Nrf2* mRNA (Fig. 7B) and protein (Fig. 7C), as well as the mRNA levels of *Nqo1* and *Ho1* (Fig. 7D). Hence, P300 was found, in the present study, to mediate NaB-induced *Nrf2* expression and function in HG-treated ECs.

Fig. 7

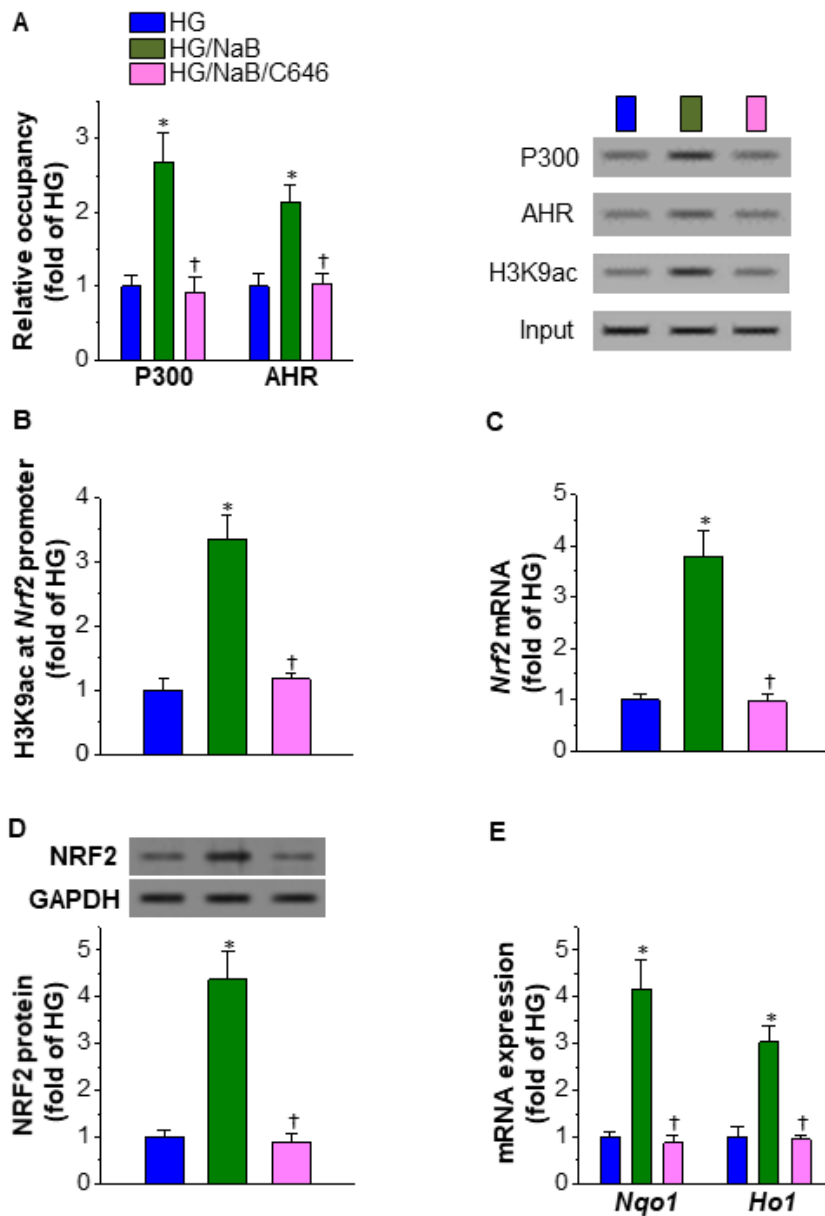


Fig. 7. P300 mediated NaB-induced activation of *Nrf2* in HG-treated ECs.

To explore whether P300 is required for NaB's activation of *Nrf2* expression and function, HG-treated ECs were co-treated with NaB, in the presence or absence of C646. (A) P300, AHR and (B) H3K9ac occupancy at the *Nrf2* gene promoter was determined by ChIP assay. *Nrf2* (C) mRNA and (D) protein levels were evaluated using RT-PCR and Western blot. The mRNA levels of (E) *Nqo1* and *Ho1* were further determined by RT-PCR. Data was normalized to HG and presented as means \pm SD (n = 3). *, $p < 0.05$ vs HG. †, $p < 0.05$ vs HG/NaB. Bars: white, HG; light grey, HG/NaB; dark grey, HG/NaB/C646. Abbreviations are the same as in Figs. 1, 3, 4, 6.

Fig. 7. P300 mediated NaB-induced activation of *Nrf2* in HG-treated ECs. To explore whether P300 is required for NaB's activation of *Nrf2* expression and function, HG-treated ECs were co-treated with NaB, in the presence or absence of C646. (A) P300, AHR and (B) H3K9ac occupancy at the *Nrf2* gene promoter was determined by ChIP assay. *Nrf2* (C) mRNA and (D) protein levels were evaluated using RT-PCR and Western blot. The mRNA levels of (E) *Nqo1* and *Ho1* were further determined by RT-PCR. Data was normalized to HG and presented as means \pm SD (n = 3). *, $p < 0.05$ vs HG. †, $p < 0.05$ vs HG/NaB. Bars: white, HG; light grey, HG/NaB; dark grey, HG/NaB/C646. Abbreviations are the same as in Figs. 1, 3, 4, 6.

3.8 P300 was required for NaB's attenuation of HG-induced oxidative stress and inflammation in ECs.

The role of P300 in NaB's protection against HG-induced oxidative stress and inflammation was further tested in HG-treated ECs, by using the P300 inhibitor C646. NaB significantly attenuated the levels of ROS (Fig. 8A, left panel) and MDA (Fig. 8A, right panel), as well as the mRNA expression of *Vcam-1* (Fig. 8B, left panel) and *Icam-1* (Fig. 8B, right panel). These effects of NaB were completely abrogated by C646 (Fig. 8A, B). These results provide an evidence for the critical role of P300 in mediating NaB's protective effects on HG-induced aortic endothelial oxidative stress and inflammation.

Fig. 8

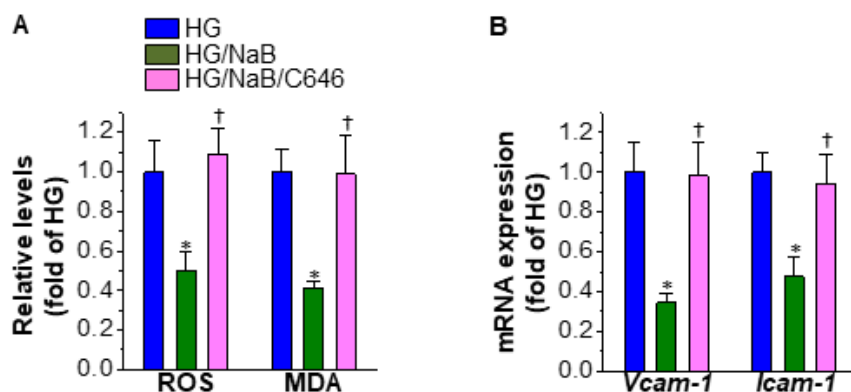


Fig. 8. P300 was required for NaB's attenuation of HG-induced oxidative stress and inflammation in ECs. In order to test whether or not P300 predominantly mediates NaB's protection against HG-induced aortic endothelial oxidative stress and inflammation, (A) ROS and (B) MDA levels, as well as the expression of *Vcam-1* and *Icam-1* mRNAs were determined in HG and NaB co-treated ECs, in the presence or absence of C646. Data was normalized to HG and presented as means \pm SD (n = 3). *, $p < 0.05$ vs HG. †, $p < 0.05$ vs HG/NaB. Bars: white, HG; light grey, HG/NaB; dark grey, HG/NaB/C646. Abbreviations are the same as in Figs. 1, 2, 4.

Fig. 8. P300 was required for NaB's attenuation of HG-induced oxidative stress and inflammation in ECs. In order to test whether or not P300 predominantly mediates NaB's protection against HG-induced aortic endothelial oxidative stress and inflammation, (A) ROS and (B) MDA levels, as well as the expression of *Vcam-1* and *Icam-1* mRNAs were determined in HG and NaB co-treated ECs, in the presence or absence of C646. Data was normalized to HG and presented as means \pm SD (n = 3). *, $p < 0.05$ vs HG. †, $p < 0.05$ vs HG/NaB. Bars: white, HG; light grey, HG/NaB; dark grey, HG/NaB/C646. Abbreviations are the same as in Figs. 1, 2, 4.

4. Discussion

Here we report NaB's protection against DM-induced aortic endothelial dysfunction. By using *Nrf2* KO mice, NRF2 was found to be essential for both self-defense and the NaB's beneficial effects. By comparing to SFN, NaB was confirmed to activate *Nrf2* at the transcription level, without facilitating NRF2 nuclear translocation. Mechanistically, NaB inhibited HDAC activity and increased AHR and P300 occupancy at the *Nrf2* promoter. Furthermore, by using C646, P300 was found to be essential in mediating NaB's effects on the activation of *Nrf2* expression and function, as well as the attenuation of oxidative stress and inflammation.

One important finding, as observed in the present study, is the distinct behaviors of NaB and SFN in regulation of *Nrf2* gene expression. SFN facilitated NRF2 nuclear translocation (Fig. 5E) without increasing *Nrf2* gene transcription (Fig. 5A). However, NaB did not trigger NRF2 nuclear translocation (Fig. 5E). Rather, it activated *Nrf2* at the transcription level (Fig. 5A), the effect of which produced abundant NRF2 protein (Fig. 5B, C) and increased the amount (Fig. 5D), but not the proportion (Fig. 5E), of n-NRF2. Hence, despite both being activators of NRF2, NaB and SFN activate NRF2 through completely different mechanisms.

Extensive studies have previously been focusing on KEAP1 inhibition, as the strategy to activate NRF2 [45-47]. However, little attention was paid to prior steps of *Nrf2* gene expression, including translation and transcription. The present study may provide histone modification as a NRF2-activating strategy, which is different from KEAP1 inhibition. In addition, transcription

factor-induced gene expression pathway also needs to be further studied. Enough attention has not been previously paid to AHR-induced *Nrf2* gene expression. As a transcription factor of NRF2, AHR activation may enhance *Nrf2* expression and function. In the present study, HDAC inhibition by NaB facilitated AHR binding at the *Nrf2* promoter (Fig. 7A, right panel), suggesting the requirement of physical space for the transcriptional machinery at the *Nrf2* promoter. Future studies will be focused on whether the increase in AHR could activate *Nrf2* transcription upon different status of the chromatin structure.

One concern for HDAC inhibition could be the possible off-target effects. Change of the chromatin structure by HDAC inhibition might possibly facilitate the expression of various genes, in addition to *Nrf2*. However, only 2% of mammalian genes are affected by HDAC inhibition [48], indicating a relatively selective effect of NaB on the alteration of the genome transcription. The action of butyrate is often mediated through Sp1/Sp3 binding sites, which recruit HDACs, within the promoters of genes, namely butyrate-responsive genes [48]. One explanation is that *Nrf2* might be a butyrate-responsive gene, whereas many other genes, probably the rest 98% of mammalian genes, might not be. Supporting this view, HDAC inhibition by NaB led to an enhanced *Nrf2* gene transcription (Fig. 7B) and a decreased *Vcam-1* and *Icam-1* gene transcription (Fig. 8B) in HG-treated ECs, as well as an unaltered *Keap1* gene transcription in both the diabetic and non-diabetic kidneys [24]. Thus, despite the decompression of the DNA, not all the tested genes positively responded to NaB. Another possible speculation could be that this relatively selective effect might be caused by HDAC inhibition-induced incomplete decompression of the chromatin structure, which prevents most genes from transcription. Further studies are needed to investigate these interesting speculations. Nonetheless, the final outcome of NaB treatment was, indeed, a mixture of the global effects produced by HDAC inhibition,

including both the beneficial and the detrimental, with the beneficial effect playing the predominant role. Additionally, since butyrate itself inhibits class I HDAC activity, specifically HDAC1, HDAC2, HDAC3 and HDAC8 [22], future studies may be performed to dissect and clarify the function of each isoform in control of *Nrf2* gene transcription. This may facilitate better understanding of the action of each isoform and may thus improve specificity in *Nrf2* activation.

NRF2 activators were tested in clinical trials [49-52], with dimethyl fumarate approved in clinical treatment of multiple sclerosis [53], demonstrating NRF2 to be a viable drug target. However, to date, no NRF2 activator has been studied in clinical trials of diabetic macrovascular complications. The fact that NaB is not only found in human food but also is produced by human intestinal fermentation [21] has granted NaB supplementation a unique advantage in safety, in future small clinical trials.

Taken together, the present study highlighted a NRF2-mediated protection by NaB against DM-induced aortic endothelial dysfunction. NaB transcriptionally activated *Nrf2* gene expression, the effect of which was mediated by P300. The present study demonstrates an epigenetic regulatory mechanism of *Nrf2* antioxidant signaling, which may be a strategy in future management of diabetic vasculopathy.

Author contributions

Hao Wu conceived the project. Hao Wu, Bin Liu and Junduo Wu designed the experiments. Junduo Wu, Hao Wu, Ziping Jiang, Haina Zhang, Wenzhao Liang, Wenlin Huang, Huan Zhang, Ying Li, Zhaohui Wang, Junnan Wang and Ye Jia researched the data. Hao Wu, Bin Liu and Junduo Wu wrote the manuscript. Hao Wu, Bin Liu, Junnan Wang, Ye Jia, Junduo Wu, Ziping

Jiang, Haina Zhang, Wenzhao Liang, Wenlin Huang, Huan Zhang, Ying Li and Zhaohui Wang stimulated discussion, reviewed and revised the manuscript. Hao Wu, Bin Liu, Ziping Jiang, Wenzhao Liang, Zhaohui Wang, Junnan Wang and Ye Jia provided funding. All the authors approve the version to be published.

Funding sources

This work was supported in part by the National Natural Science Foundation of China [81600573] and Norman Bethune Program of Jilin University [2015438] to Hao Wu; National Natural Science Foundation of China (81570250) and Department of Science and Technology of Jilin Province (201603059YY; 20150204008YY) to Bin Liu; Natural Science Foundation of Jilin Province [2018SCZWSZX-045] to Ziping Jiang; National Natural Science Foundation of China [81700393] to Wenzhao Liang; National Natural Science Foundation of China [81774393] to Zhaohui Wang; Department of Science and Technology of Jilin Province [20170204032YY] and Development and Reform Commission of Jilin Province [2014G072] to Junnan Wang; and Research Program of Jilin University [3R2173203428] to Ye Jia.

Declarations of interest

None.

References

1. Forbes, J.M., et al., *Advanced glycation end product interventions reduce diabetes-accelerated atherosclerosis*. *Diabetes*, 2004. **53**(7): p. 1813-23.

2. King, G.L. and H. Wakasaki, *Theoretical mechanisms by which hyperglycemia and insulin resistance could cause cardiovascular diseases in diabetes*. *Diabetes Care*, 1999. **22 Suppl 3**: p. C31-7.
3. Giovannini, P., M.J. Howes, and S.E. Edwards, *Medicinal plants used in the traditional management of diabetes and its sequelae in Central America: A review*. *J Ethnopharmacol*, 2016. **184**: p. 58-71.
4. Meek, T.H. and G.J. Morton, *The role of leptin in diabetes: metabolic effects*. *Diabetologia*, 2016. **59**(5): p. 928-32.
5. Sharma, A., et al., *The nuclear factor (erythroid-derived 2)-like 2 (Nrf2) activator dh404 protects against diabetes-induced endothelial dysfunction*. *Cardiovasc Diabetol*, 2017. **16**(1): p. 33.
6. Basta, G., et al., *At least 2 distinct pathways generating reactive oxygen species mediate vascular cell adhesion molecule-1 induction by advanced glycation end products*. *Arterioscler Thromb Vasc Biol*, 2005. **25**(7): p. 1401-7.
7. Hulsmans, M. and P. Holvoet, *The vicious circle between oxidative stress and inflammation in atherosclerosis*. *J Cell Mol Med*, 2010. **14**(1-2): p. 70-8.
8. Mittal, M., et al., *Reactive oxygen species in inflammation and tissue injury*. *Antioxid Redox Signal*, 2014. **20**(7): p. 1126-67.
9. Basta, G., A.M. Schmidt, and R. De Caterina, *Advanced glycation end products and vascular inflammation: implications for accelerated atherosclerosis in diabetes*. *Cardiovasc Res*, 2004. **63**(4): p. 582-92.
10. Kaspar, J.W., S.K. Niture, and A.K. Jaiswal, *Nrf2:INrf2 (Keap1) signaling in oxidative stress*. *Free Radic Biol Med*, 2009. **47**(9): p. 1304-9.

11. Zheng, H., et al., *Therapeutic potential of Nrf2 activators in streptozotocin-induced diabetic nephropathy*. *Diabetes*, 2011. **60**(11): p. 3055-66.
12. Ruiz, S., et al., *Targeting the transcription factor Nrf2 to ameliorate oxidative stress and inflammation in chronic kidney disease*. *Kidney Int*, 2013. **83**(6): p. 1029-41.
13. Zhang, D.D. and M. Hannink, *Distinct cysteine residues in Keap1 are required for Keap1-dependent ubiquitination of Nrf2 and for stabilization of Nrf2 by chemopreventive agents and oxidative stress*. *Mol Cell Biol*, 2003. **23**(22): p. 8137-51.
14. Gu, J., et al., *Metallothionein is Downstream of Nrf2 and Partially Mediates Sulforaphane Prevention of Diabetic Cardiomyopathy*. *Diabetes*, 2016.
15. He, X., et al., *Nrf2 is critical in defense against high glucose-induced oxidative damage in cardiomyocytes*. *J Mol Cell Cardiol*, 2009. **46**(1): p. 47-58.
16. Jiang, T., et al., *The protective role of Nrf2 in streptozotocin-induced diabetic nephropathy*. *Diabetes*, 2010. **59**(4): p. 850-60.
17. Wu, H., et al., *Metallothionein plays a prominent role in the prevention of diabetic nephropathy by sulforaphane via up-regulation of Nrf2*. *Free Radic Biol Med*, 2015. **89**: p. 431-442.
18. Wu, H., et al., *C66 ameliorates diabetic nephropathy in mice by both upregulating NRF2 function via increase in miR-200a and inhibiting miR-21*. *Diabetologia*, 2016. **59**(7): p. 1558-68.
19. Wang, Y., et al., *Sulforaphane attenuation of type 2 diabetes-induced aortic damage was associated with the upregulation of Nrf2 expression and function*. *Oxid Med Cell Longev*, 2014. **2014**: p. 123963.

20. Ha, C.M., et al., *Activation of Nrf2 by dimethyl fumarate improves vascular calcification*. *Vascul Pharmacol*, 2014. **63**(1): p. 29-36.
21. Li, H., et al., *Sodium butyrate stimulates expression of fibroblast growth factor 21 in liver by inhibition of histone deacetylase 3*. *Diabetes*, 2012. **61**(4): p. 797-806.
22. Candido, E.P., R. Reeves, and J.R. Davie, *Sodium butyrate inhibits histone deacetylation in cultured cells*. *Cell*, 1978. **14**(1): p. 105-13.
23. Yaku, K., et al., *The enhancement of phase 2 enzyme activities by sodium butyrate in normal intestinal epithelial cells is associated with Nrf2 and p53*. *Mol Cell Biochem*, 2012. **370**(1-2): p. 7-14.
24. Dong, W., et al., *Sodium butyrate activates NRF2 to ameliorate diabetic nephropathy possibly via inhibition of HDAC*. *J Endocrinol*, 2017. **232**(1): p. 71-83.
25. Roth, S.Y., J.M. Denu, and C.D. Allis, *Histone acetyltransferases*. *Annu Rev Biochem*, 2001. **70**: p. 81-120.
26. Narlikar, G.J., H.Y. Fan, and R.E. Kingston, *Cooperation between complexes that regulate chromatin structure and transcription*. *Cell*, 2002. **108**(4): p. 475-87.
27. Miao, W., et al., *Transcriptional regulation of NF-E2 p45-related factor (NRF2) expression by the aryl hydrocarbon receptor-xenobiotic response element signaling pathway: direct cross-talk between phase I and II drug-metabolizing enzymes*. *J Biol Chem*, 2005. **280**(21): p. 20340-8.
28. Bowers, E.M., et al., *Virtual ligand screening of the p300/CBP histone acetyltransferase: identification of a selective small molecule inhibitor*. *Chem Biol*, 2010. **17**(5): p. 471-82.
29. Sun, W., et al., *Epigallocatechin Gallate Upregulates NRF2 to Prevent Diabetic Nephropathy via Disabling KEAP1*. *Free Radic Biol Med*, 2017.

30. Kato, M., et al., *An endoplasmic reticulum stress-regulated lncRNA hosting a microRNA megacluster induces early features of diabetic nephropathy*. Nat Commun, 2016. **7**: p. 12864.
31. Gao, Z., et al., *Butyrate improves insulin sensitivity and increases energy expenditure in mice*. Diabetes, 2009. **58**(7): p. 1509-17.
32. Pan, C., et al., *NRF2 Plays a Critical Role in Both Self and EGCG Protection against Diabetic Testicular Damage*. Oxid Med Cell Longev, 2017. **2017**: p. 3172692.
33. Wu, H., et al., *Metallothionein deletion exacerbates intermittent hypoxia-induced renal injury in mice*. Toxicol Lett, 2014. **232**(2): p. 340-348.
34. Kobayashi, M., et al., *A simple method of isolating mouse aortic endothelial cells*. J Atheroscler Thromb, 2005. **12**(3): p. 138-42.
35. Aguilar, E.C., et al., *Butyrate impairs atherogenesis by reducing plaque inflammation and vulnerability and decreasing NFkappaB activation*. Nutr Metab Cardiovasc Dis, 2014. **24**(6): p. 606-13.
36. Kooistra, T., et al., *Butyrate stimulates tissue-type plasminogen-activator synthesis in cultured human endothelial cells*. Biochem J, 1987. **247**(3): p. 605-12.
37. Ciura, J. and P.P. Jagodzinski, *Butyrate increases the formation of anti-angiogenic vascular endothelial growth factor variants in human lung microvascular endothelial cells*. Mol Biol Rep, 2010. **37**(8): p. 3729-34.
38. Ishikado, A., et al., *Willow bark extract increases antioxidant enzymes and reduces oxidative stress through activation of Nrf2 in vascular endothelial cells and Caenorhabditis elegans*. Free Radic Biol Med, 2013. **65**: p. 1506-15.

39. Campbell, L., et al., *Selenium and sulforaphane modify the expression of selenoenzymes in the human endothelial cell line EAhy926 and protect cells from oxidative damage*. Nutrition, 2007. **23**(2): p. 138-44.
40. Shan, Y., et al., *Protective effect of sulforaphane on human vascular endothelial cells against lipopolysaccharide-induced inflammatory damage*. Cardiovasc Toxicol, 2010. **10**(2): p. 139-45.
41. Cho, Y.S., et al., *Inhibition of STAT3 phosphorylation by sulforaphane reduces adhesion molecule expression in vascular endothelial cell*. Can J Physiol Pharmacol, 2015: p. 1-7.
42. Wu, H., et al., *SRT2104 attenuates diabetes-induced aortic endothelial dysfunction via inhibition of P53*. J Endocrinol, 2018. **237**(1): p. 1-14.
43. Miao, X., et al., *Therapeutic effect of MG132 on the aortic oxidative damage and inflammatory response in OVE26 type 1 diabetic mice*. Oxid Med Cell Longev, 2013. **2013**: p. 879516.
44. Liu, Y., et al., *Inhibition of JNK by compound C66 prevents pathological changes of the aorta in STZ-induced diabetes*. J Cell Mol Med, 2014. **18**(6): p. 1203-12.
45. Suzuki, T. and M. Yamamoto, *Stress-sensing mechanisms and the physiological roles of the Keap1-Nrf2 system during cellular stress*. J Biol Chem, 2017. **292**(41): p. 16817-16824.
46. Canning, P., F.J. Sorrell, and A.N. Bullock, *Structural basis of Keap1 interactions with Nrf2*. Free Radic Biol Med, 2015. **88**(Pt B): p. 101-107.
47. Uruno, A., Y. Yagishita, and M. Yamamoto, *The Keap1-Nrf2 system and diabetes mellitus*. Arch Biochem Biophys, 2015. **566**: p. 76-84.

48. Davie, J.R., *Inhibition of histone deacetylase activity by butyrate*. J Nutr, 2003. **133**(7 Suppl): p. 2485S-2493S.
49. Pergola, P.E., et al., *Effect of bardoxolone methyl on kidney function in patients with T2D and Stage 3b-4 CKD*. Am J Nephrol, 2011. **33**(5): p. 469-76.
50. Brown, R.H., et al., *Sulforaphane improves the bronchoprotective response in asthmatics through Nrf2-mediated gene pathways*. Respir Res, 2015. **16**: p. 106.
51. Kikuchi, M., et al., *Sulforaphane-rich broccoli sprout extract improves hepatic abnormalities in male subjects*. World J Gastroenterol, 2015. **21**(43): p. 12457-67.
52. Yanaka, A., et al., *Dietary sulforaphane-rich broccoli sprouts reduce colonization and attenuate gastritis in Helicobacter pylori-infected mice and humans*. Cancer Prev Res (Phila), 2009. **2**(4): p. 353-60.
53. Gold, R., et al., *Placebo-controlled phase 3 study of oral BG-12 for relapsing multiple sclerosis*. N Engl J Med, 2012. **367**(12): p. 1098-107.

Highlights

- NRF2 is critical in self-defense and NaB's protection against diabetes-induced aortic endothelial dysfunction.
- NaB activates *Nrf2* expression at the transcription level.
- P300 is required for NaB's effects on *Nrf2* activation and endothelial protection.